CrystEngComm

PAPER

Check for updates

Cite this: CrystEngComm, 2018, 20, 6310

Influence of lithium and magnesium on the real structure and dielectric properties of $Ca_9Y(VO_4)_7$ single crystals

Bogdan Lazoryak, [a] Dina Deyneko, *[a] Sergey Aksenov, [b] Vadim Grebenev, [b] Sergey Stefanovich, [a] Konstantin Belikov, [c] Miron Kosmyna, [c] Alexey Shekhovtsov, [c] Adrian Sulich [d] and Wojciech Paszkowicz [d]

Received 27th July 2018, Accepted 13th September 2018

DOI: 10.1039/c8ce01252k

rsc.li/crystengcomm

Grown by the Czochralski method, pure magnesium and lithium doped $Ca_9Y(VO_4)_7$ single crystals ($Ca_9Y(VO_4)_7$ (**C1**), $Ca_9Y(VO_4)_7$:Li (**C2**) and $Ca_9Y(VO_4)_7$:Mg (**C3**), respectively) are characterized by means of chemical analysis, X-ray diffraction analysis and high-temperature dielectric spectroscopy. All crystals demonstrate good structural performance with almost isotropic micromosaics, free of extended defects and mechanical stress. Evidences for mobile domain structure are observed below the ferroelectric Curie temperature at 1213 ± 5 K. The temperatures of ferroelectric-paraelectric phase transitions in $Ca_9Y(VO_4)_7$, $Ca_9Y(VO_4)_7$:Li and $Ca_9Y(VO_4)_7$:Mg almost coincide. In the paraelectric phase in these crystals, there is another phase transition at 1293 ± 5 K. The electrical nature and temperatures of both transitions are in agreement with the sequence of phases $R3c \rightarrow R\bar{3}c \rightarrow R\bar{3}m$ earlier suggested to occur at the same temperatures in $Ca_9Y(VO_4)_7$ on the basis of other experimental evidences. In all temperature modifications of $R3c$, $R\bar{3}c$, and $R\bar{3}m$, the $Ca_9Y(VO_4)_7$:Li crystal has the highest activation energy and two-orders lower Ca^{2+} ionic conductivity in comparison with nominally pure $Ca_9Y(VO_4)_7$ with the conductivity of $Ca_9Y(VO_4)_7$:Mg lying in between. The observed influence of guest atoms is connected with different structural roles of lithium and magnesium in whitlockite crystal lattices where atoms of lithium all reside in unique M4 atomic sites crossing ion-conduction pathways. Magnesium atoms iso-structurally substitute for calcium in position M5 and have a smaller effect on fast Ca^{2+} transport.

1. Introduction

$Ca_3(VO_4)_3$ has a polar crystal structure and belongs to the whitlockite family of minerals and their synthetic analogues. Since the non-centrosymmetric and ferroelectric properties of a Czochralski-grown $Ca_3(VO_4)_3$ were reported forty years ago,[1] a number of $Ca_9R(VO_4)_7$ (R = REE, Y or Bi) crystals with a similar structure have already demonstrated their potentials for laser and non-linear optic applications in the near IR-region.[2–10] In addition to these crystals, the whitlockite family contains many other substances differing in cationic and anionic compositions and possessing a variety of properties including high-temperature ferroelectricity, second-order optical nonlinearity, ionic conductivity, and luminescence.[11–14] Some of them may be utilized as useful additives modifying the properties of $Ca_9R(VO_4)_7$ crystals in the desired direction. In particular, it was determined that the diffusion of Pb^{2+} into $Ca_9Bi(VO_4)_7$ greatly enhances its activity in optical second harmonic generation and lowers the ferroelectric Curie temperature from 1075 K to approximately 750 K.[11] Substitutions with Mg, Zn or Cd for Ca drastically reduces the Ca^{2+} ionic conductivity of the compounds.[15,16] In the promising ferroelectric laser single crystal $Ca_9Y(VO_4)_7$, replacing half of the vanadium with phosphorus stabilizes the paraelectric phase, which gave an example of whitlockite structure with a centre of symmetry. Due to the absence of a ferroelectric domain structure, the centro-symmetric crystals $Ca_9Y(P_xV_{1-x}O_4)_7$ exhibited lower light scattering and better transparency.[17]

The dependence of ionic conductivity, non-linear optical and luminescence properties on chemical composition and the distribution of cations over the M1–M5 crystallographic sites of the whitlockite-type structure have been investigated.[5,16–20] It has been shown that these properties are very sensitive to the presence of certain cations in M1–M5 sites. This strategy is used for the targeted properties modification of $Ca_9R(VO_4)_7$ (R = REE, Y or Bi) single crystals.

[a] Chemistry Department, Moscow State University, Moscow, 119991, Russia. E-mail: deynekomsu@gmail.com
[b] FSRC "Crystallography and Photonics" RAS, 59 Leninskii pr, Moscow, 119333, Russia
[c] Institute for Single Crystals, NAS of Ukraine, 60 Nauky Ave., Kharkov, 61001, Ukraine
[d] Institute of Physics, Polish Academy of Sciences, 32/46 Aleja Lotnikow, Warsaw, PL-02668, Poland

Despite intense efforts to produce high-quality single crystals of $Ca_9Y(VO_4)_7$, their optical qualities are still insufficient for nonlinear optics and laser applications because of the scattering centers. The mechanism of scattering center formation is unclear and can be connected either with redistribution of cations and cationic vacancies during high-temperature ferroelectric phase transitions or minimization of internal stresses during the cooling of crystals. According to the site-occupation scheme for $Ca_9Gd(VO_4)_7$ proposed in[20] a tendency of the Czochralski-grown $Ca_9Gd(VO_4)_7$ crystal to adopt a Gd-deficient composition was demonstrated.[20] Another origin of light scattering is related to the domain formation. There is a strong necessity to remove the 180 degree domain walls inevitably existing in these one-axis ferroelectric crystals with high Curie temperatures close to or above 1273 K.[21] As shown in the structure of $Ca_9R(VO_4)_7$,[22] large (light) R cations (La, Pr, Nd…) partially occupy all of the M1, M2 and M3 sites, whereas for small (heavy) R cations (Lu, Yb, Tm…) partially occupy of the M1 and M2 site, site M3 is exclusively occupied by Ca for small R cations. For example, the Czochralski-grown whitlockite-type crystals of $Ca_9Yb(VO_4)_7$ (ref. 21) and $Ca_9Y(VO_4)_7$ (ref. 23) show that the trivalent cations (Yb^{3+} or Y^{3+}) share with calcium M1, M2 and M5 sites, calcium cations completely occupy the M3 site, while M4 and M6 sites are empty.

In the high-temperature region of both $Ca_9Yb(VO_4)_7$ (ref. 21) and $Ca_9Y(VO_4)_7$,[23] compounds demonstrate the presence of two phase transitions. The lower temperature ones were accompanied by distinct dielectric anomalies of ferroelectric type at about 1221 and 1219 K, correspondingly, the higher-temperature phase transitions at 1276 and 1293 K were referred to superstructural changes in crystal lattices. Differential thermal analysis (DTA) confirmed the existence of similar phase transitions in the crystals grown from the melts containing lithium ($Ca_9Y(VO_4)_7$:Li) or magnesium ($Ca_9Y(VO_4)$:Mg). The comparison between nominally pure $Ca_9Y(VO_4)_7$ crystals and lithium- or magnesium-doped ones reported in ref. 23 revealed either the absence or minor influence of impurity cations on the crystal structure parameters and phase transitions. Namely, only a small amount of Mg^{2+}cations were detected[23] in the octahedral M5 site that was accompanied with a barely noticeable decrease in temperature of the ferroelectric-paraelectric phase transition from T_c = 1219 K to 1217 K. A very close Curie temperature T_c = 1208 K was also found with DTA for $Ca_9Y(VO_4)_7$:Li. There was no indication of guest atoms present in the latter crystal during X-ray single crystal structure investigation.[23]

In this study, we use X-ray diffraction techniques and dielectric spectroscopy to elucidate the roles of extended structural imperfections on both point defects and impurity-containing crystals of $Ca_9Y(VO_4)_7$.

2. Experimental

2.1. Synthesis and crystal growth

The previously synthesized powder $Ca_9Y(VO_4)_7$ from $CaCO_3$ (99.99%), V_2O_5 (99.95%), Y_2O_3 (99.99%) was used for growing $Ca_9Y(VO_4)_7$ (**C1**), $Ca_9Y(VO_4)_7$:Li (**C2**) and $Ca_9Y(VO_4)_7$:Mg (**C3**) single crystals. Some details of synthesis conditions, chemical composition of single crystals **C1**, **C2** and **C3** have been previously described.[23]

The Czochralski method was used for crystal growth of pure and doped crystals. The crystal growth was carried out in an argon atmosphere using Ir crucibles by means of "Kristall 3M" setup equipped with inductive heating and an automated control diameter system. The pulling rate was tuned within 1–5 mm h^{-1} and the rotation rate was varied in the range of 5–25 rpm. Both active and passive after-heaters were employed. In the crystallization unit, the radial temperature gradient on surface of the melt did not exceed 0.5 deg mm^{-1}; axial temperature gradient at the melt–argon interface was 75 deg cm^{-1}. The crystal–melt interface was convex. The direction of the growing crystals was [001]. All crystals were grown under the same conditions, at fixed gradients, pulling and rotation rates. To minimize thermoelastic stresses, after the detachment of crystals, the ingots were kept above the melt for 2 h and cooled down to room temperature for 24 h. Additionally, the crystals were annealed in air at 1273 K for 12 h at the heating/cooling rate 50 deg h^{-1}. The typical dimensions of crystals were: diameter – up to 25 mm, length – up to 70 mm.

Li_2CO_3 and MgO were added in the synthesized charge over the stoichiometric ratio. The lithium and magnesium concentrations in the charge were 0.245 and 0.2 wt%, respectively. The samples for investigations were cut from the central part of each crystal.

2.2. Chemical composition

The chemical composition of the single crystal **C1** investigated in[23] was found to correspond to stoichiometric $Ca_9Y(VO_4)_7$. Both chemical and single crystal X-ray analysis confirmed the composition of $Ca_9Y(VO_4)$:Mg to correspond to $Ca_{8.854}Mg_{0.145}Y(VO_4)_7$. Special attention in this study was paid to lithium content refinement in crystal **C2** due to its minor influence on crystal structure and phase transition according to data in ref. 23.

Lithium content in the crystals was determined by means of inductively-coupled plasma atomic emission spectrometry using a Thermo Scientific iCAP 6300 Duo spectrometer. For the study, the crystal was ground in agate mortar and the resulting fine powder was dissolved in condensed phosphoric acid. Lithium concentration was measured by the method of standard additions. The following operating conditions were used: RF power – 950 W, solution uptake rate – 2 mL min^{-1}, plasma view – radial, analytical wavelength – 670.784 nm. Experiments were run in triplicate with relative standard error less than 2%. The probes from three areas of the crystal were selected for measurements. Since the length of crystal was about 70 mm, the pieces from the top, center (30 mm from the top of crystal) and bottom were cut from the crystal and dissolved.

A gradient of Li content was observed along the crystal (Table 1). The weight fraction of lithium in the central part of

Table 1 Lithium distribution along the grown boule of $Ca_9Y(VO_4)_7$ single crystal[a]

$Ca_9Y(VO_4)_7$:Li	Li concentration, wt%
Top*	0.054
Center	0.065
Bottom	0.072

[a] The length of crystal was about 70 mm. "Center" means 30 mm from the top of crystal.

crystal $Ca_9Y(VO_4)_7$:Li corresponds to the chemical formula $Ca_{8.93}Li_{0.14}Y(VO_4)_7$.

2.3. Methods of investigation

Crystals of $Ca_9Y(VO_4)_7$, $Ca_9Y(VO_4)_7$:Li and $Ca_9Y(VO_4)_7$:Mg were selected carefully under a polarizing microscope and used for single-crystal X-ray data collection. The single-crystal X-ray data were collected at room temperature on a STOE Stadi Vari-PILATUS-100K diffractometer with graphite monochromatized MoK_α radiation (λ = 0.71073 Å) and a CCD detector using the ω/φ-scanning mode. Raw data were integrated and then scaled, merged, and corrected for Lorentz-polarization effects using the WinGX pack.[24] The structure refinement was carried out using the Jana2006 program package.[25]

The optical transmittance spectra were investigated by means of a UV-vis Perkin-Elmer spectrometer (spectral range 190–1100 nm). The photo of as-grown crystals and their optical transmittance spectra are given in Fig. 1.

The method of real structure investigations of single crystals was described in detail in a previous report.[26] A high-resolution Philips X'Pert diffractometer equipped with a standard laboratory source of $CuK_{\alpha 1}$ radiation (λ = 1.54056 Å) was applied to study the defect structure of the single crystals **C1**, **C2** and **C3**. X-ray rocking curves as well as reciprocal space maps (RSM) of reflection 0 0 30 were obtained to characterize diffuse scattering and evaluate their crystallographic quality.

The dielectric properties were measured on crystal plates cut perpendicular to the polar axis of the boules. The plates had flat surfaces of about 60 mm^2 and were 1–2 mm thick. The large surfaces of plates were covered with Pt paint (SpiChem). The paint did not need any heat treatment to produce conductive electrodes with dc-electrical resistivity less than 1 Ohm. The dielectric measurements were fulfilled in the frequency range of 0.1 Hz–14 MHz at stepwise heating–cooling cycles with the average rate of 0.9 K min^{-1} in air. A Novocontrol Alpha-ANT impedance analyzer supplied with ZG4 interface and double-contact ProboStat measuring cell was used.

Static bulk conductivity was calculated from complex impedance Z^* by means of an equivalent electrical circuits routine. For each sample, the data obtained on heating are in good agreement with those obtained in cooling, thus pointing to equilibrium conditions in the course of dielectric experiments. Taking this into account, the standard impedance Z^* approximation was produced only in cooling. The equivalent electric circuit in Fig. 1 was used, where R stands for bulk resistance of the sample, CPE = $1/[Q(j\omega)^n]$ – constant phase element which was introduced in calculations for better data approximation, Q and n being frequency independent. The exponential factor n was determined to be in the range of 0.88–0.98, a Q_o of about 2 pF responded to the geometrical capacitance of the measurement cell. Impedance data for three temperatures for all samples are shown as an example in Fig. 2. Static bulk resistance was recalculated to be presented as direct-current conductivity, σ_{dc}.

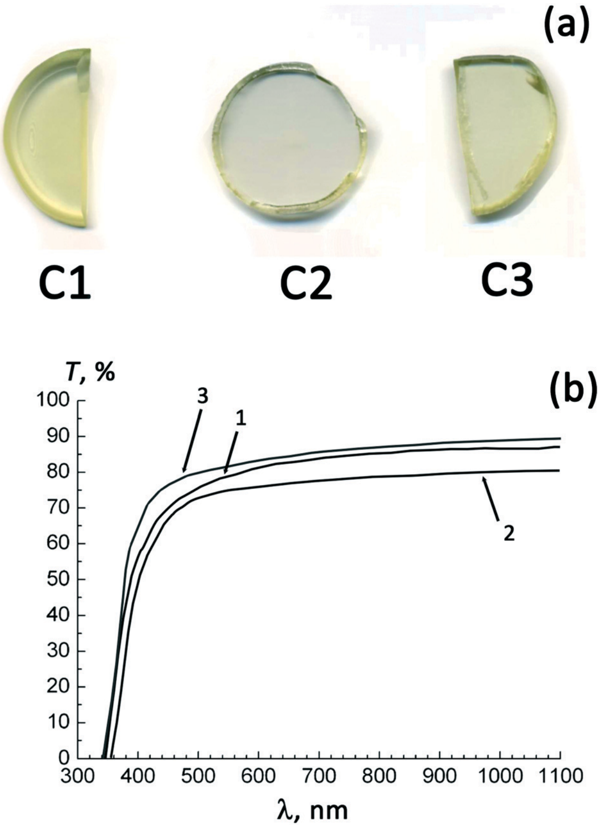

Fig. 1 The photo of as-grown **C1**, **C2**, **C3** single crystals (a) and optical transmittance spectra (b).

3. Results discussion

3.1. Quality of crystals

Crystal structures of **C1–C3** were previously published.[23] It was shown that their structures are similar to those reported for natural and synthetic members. The structures are three-dimensional and consist of layers. Between the layers, the calcium transfer is carried out through the M4 sites, which can be either empty or partially occupied by calcium, as well as other mono- and divalent cations. The impurity of Mg^{2+} cations in the structure of compound **C3** have been detected in the M5-site. However, the lithium cations were not localized in the case of X-ray structural examination because of

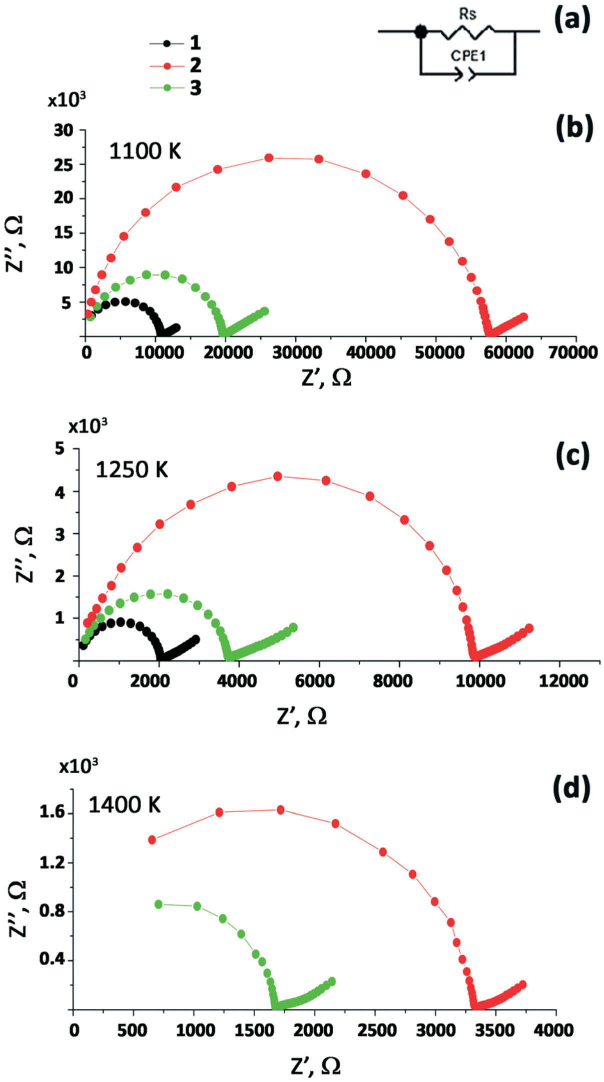

Fig. 2 Equivalent electric circuit for calculating the dielectric constant and dc-conductivity (a) and experimental impedance Z^* at 1100 K (a), 1250 K (b) and 1400 K (c) for $Ca_9Y(VO_4)_7$ (1), $Ca_9Y(VO_4)_7$:Mg (2) and $Ca_9Y(VO_4)_7$:Li (3) single crystals.

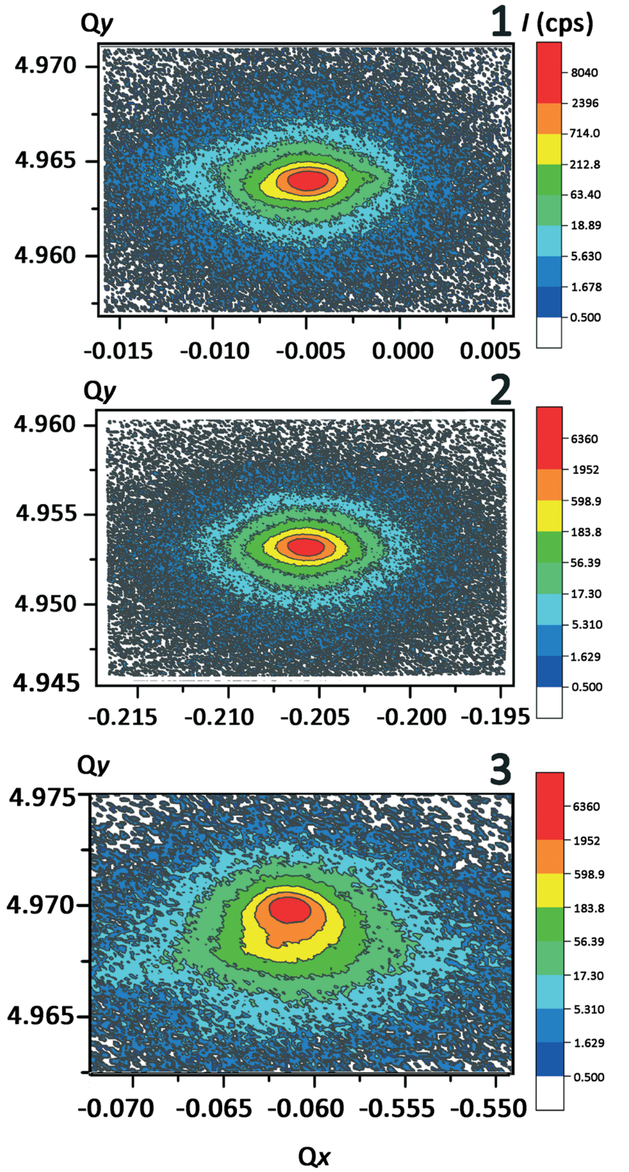

Fig. 3 Reciprocal space maps of the 0 0 30 reflection for $Ca_9Y(VO_4)_7$ (1), $Ca_9Y(VO_4)_7$:Li (2) and $Ca_9Y(VO_4)_7$:Mg (3) single crystals (from top to bottom); X-ray intensity is shown in counts per second [cps].

their small amount and weak scattering ability. In the present study, the position of lithium cations is discussed on the basis of their influence on the conductivity of the crystals and the real structure performance.

Both the regular shape of reciprocal space maps having no additional nodes (Fig. 3) and a relatively low value of the full width at half maximum (FWHM) of the rocking curves for symmetric 0 0 30 reflections (Table 2), are evidence of the high quality of the crystals. No splitting of the RSMs and rocking curves is observed, showing that there is neither a block nor macromosaic structure within the irradiated area. The rocking-curve FWHMs are approximately 80 arcsec (see Table 2). The RSMs of the 0 0 30 reflection for all the examined crystals exhibit broadening only in the Q_X direction. The lack of broadening in the Q_Z direction means that there is no lattice parameter variation in the irradiated area, which suggests that the chemical composition is uniform. The nodes tend to be elliptical (FWHM of the nodes in the Q_X direction is about twice as large as in Q_Z, see Fig. 3). This type of broadening may be attributed either to the presence of a micromosaic or to a small curvature of the (001) crystallographic plane. In summary, the formation of the nodes implies that within the irradiated area of the sample (several mm^2), the three crystals are structurally and compositionally homogeneous. However, among the three crystals, the plate of $Ca_9Y(VO_4)_7$:Mg shows a slightly different defect structure as observed at the level of the diffuse scattering. Namely, contrary to other crystals, the RSM for $Ca_{8.854}Mg_{0.145}Y(VO_4)_7$ takes more place in the reciprocal space, its shape being markedly asymmetric along the Q_Z direction (Fig. 3). The fact that the center of the diffusion-scattering part of the node in the case of $Ca_{8.854}Mg_{0.145}Y(VO_4)_7$ is located below the Bragg node, may

Table 2 Unit cell parameters and rocking-curve FWHM of pure and doped $Ca_9Y(VO_4)$ single crystals

Crystal	Unit cell parameters a, Å	c, Å	V, Å^3	Rocking-curve FWHM, arcsec
$Ca_9Y(VO_4)_7$ (**C1**)	10.8552(1)	38.0373(2)	3881.65(1)	83(3)
$Ca_9Y(VO_4)_7$:Li (**C2**)	10.8570(1)	38.0161(3)	3880.77(4)	83(3)
$Ca_9Y(VO_4)_7$:Mg (**C3**)	10.8465(1)	38.0366(2)	3875.36(3)	76(3)

be attributed to a lattice strain probably caused by the presence of microdefects (fine clusters or inclusions) in the crystal matrix, similar to related observations reported for some single crystals of other compositions.[17–19]

3.2. Dielectric properties and electric conductivity

The dependence of the dielectric permittivity (ε') on the temperature for the single crystals **C1–C3** is shown in Fig. 4. The behavior of dielectric permittivity $\varepsilon'(T)$ and loss tangent curve ($\tan\delta$) is identical for all compositions over heating and cooling cycles. The temperature position of each dielectric maximum does not depend on frequency. A sharp maximum on the dielectric permittivity ε'(T) curve is observed in the temperature range of the first phase transition T_1 = 1213 ± 5 K, evidently of ferroelectric nature. This temperature is considered here as the ferroelectric Curie temperature T_c. The second phase transition at T_2 = 1293 ± 5 K is not noticeable on the $\varepsilon'(T)$ curves but is clearly observable in the case of their reciprocal, $1/\varepsilon'(T)$, presented in Fig. 5 where it is marked with a sudden break of the curves. The temperatures of both anomalies are close to the temperatures of the first (T_1) and the second (T_2) phase transitions established by the DTA method for single crystals **C1**, **C2** and **C3** in ref. 23.

A sharp maximum of the dielectric constant in whitlockite-type compounds is common to both ferroelectric[12,13] and antiferroelectric[27] substances. However, these substances differ in respect to the domain structure which is only attributed to ferroelectrics. In order to distinguish the two types of electric polarization in the materials, the temperature dependence of the loss tangent ($\tan\delta$) was measured for all of the crystals (Fig. 6). The existence of a maximum for all studied crystals below T_c confirms the ferroelectric nature of this phase transition. An abnormal change of $\tan\delta(T)$ detected below T_c (Fig. 6) is generally observed in ferroelectrics and reflects the increasing mobility of domain walls when approaching the temperature of their disappearance, T_c.

The phase transition at T_c also manifests itself through an electrical conductivity anomaly in the form of a flexure on $\log\sigma T$ ($1/T$) dependences for all of the crystals under examination (Fig. 7), with the temperature of these flexures coinciding with T_c. Another series of the flexures in Fig. 7 corresponds to a second phase transition at T_2. The temperature dependencies of σ_{dc} in Arrhenius coordinates allowed us to calculate the energy of activation of electrical conductivity for each phase from linear portions of $\log\sigma T$ ($1/T$) curves (Table 3).

For each sample, three linear portions are observed in Fig. 7 corresponding to three phases between two phase transitions (marked by lines in Fig. 7) determined earlier with

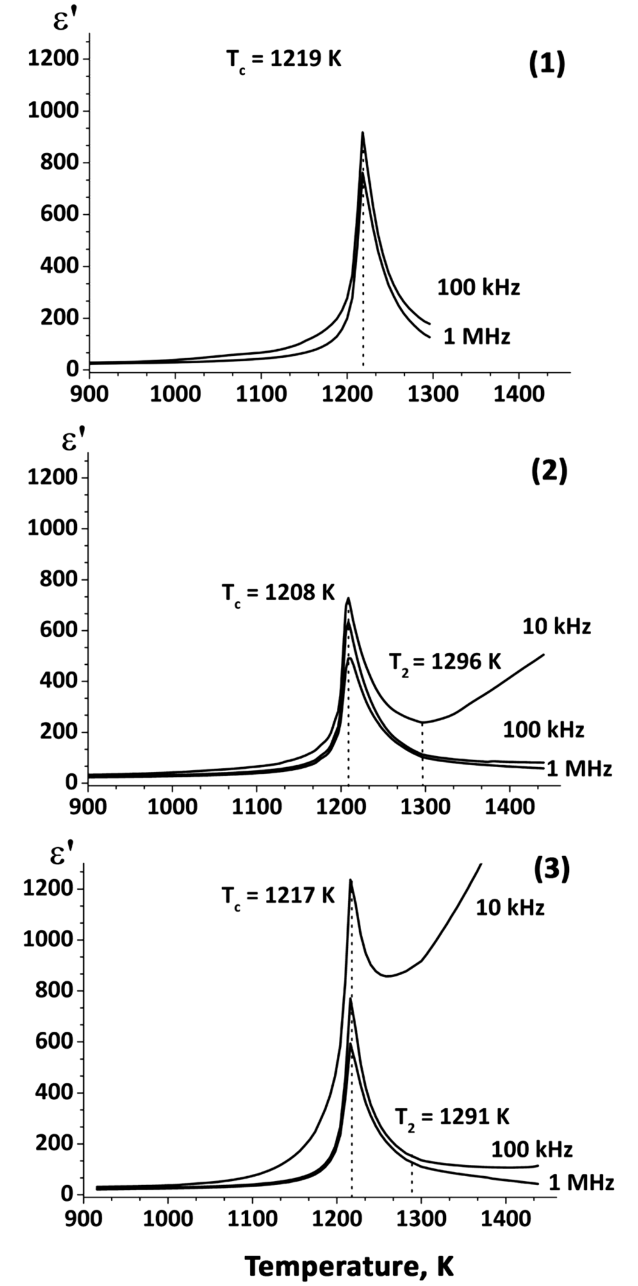

Fig. 4 Dielectric constant (ε') for crystals $Ca_9Y(VO_4)_7$ (1), $Ca_9Y(VO_4)_7$:Li (2) and $Ca_9Y(VO_4)_7$:Mg (3) with dependence on temperature at different electric field frequencies.

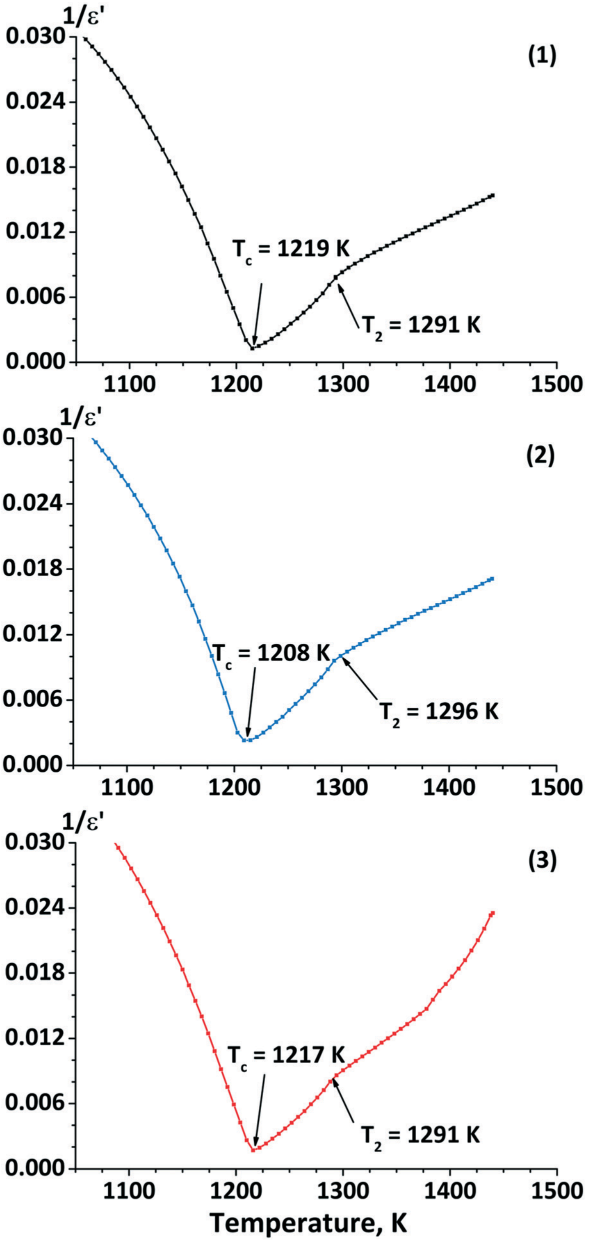

Fig. 5 Temperature dependences of reciprocal dielectric constant $1/\varepsilon'$ at frequency of 1 MHz for crystals $Ca_9Y(VO_4)_7$ (1), $Ca_9Y(VO_4)_7$:Li (2) and $Ca_9Y(VO_4)_7$:Mg (3).

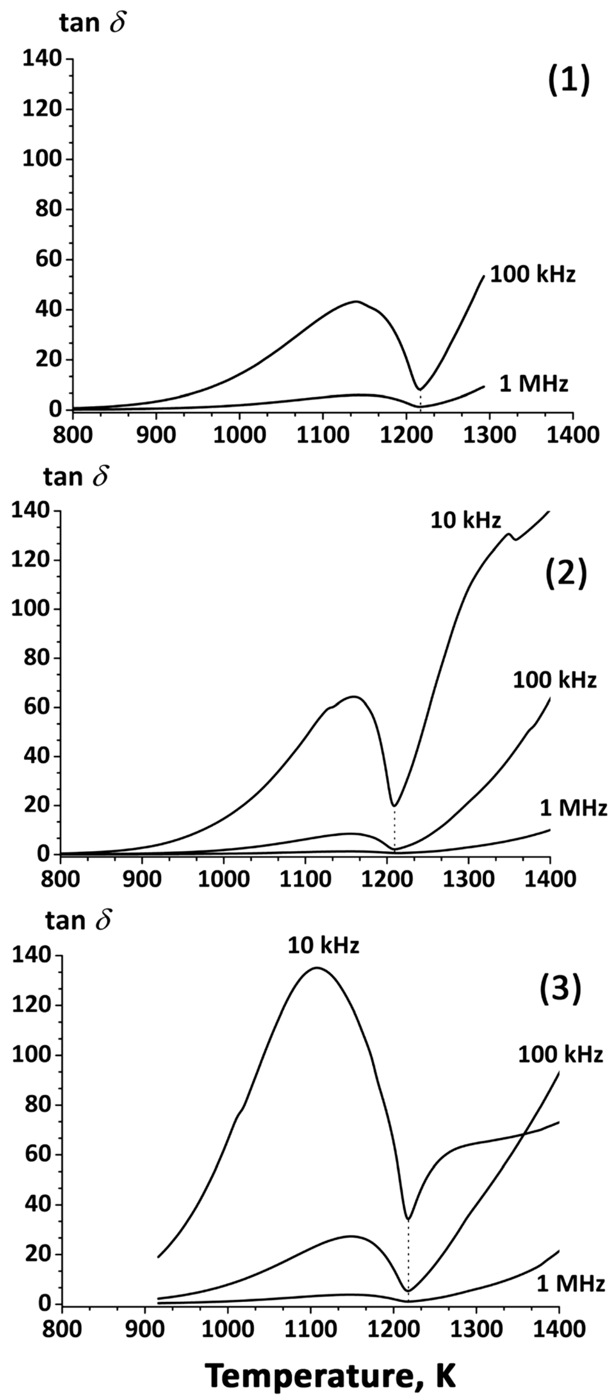

Fig. 6 The temperature dependence of $\tan\delta$ for crystals $Ca_9Y(VO_4)_7$ (1), $Ca_9Y(VO_4)_7$:Li (2) and $Ca_9Y(VO_4)_7$:Mg (3).

DTA. The temperature marked by the line at 1213 K coincides with the ferroelectric phase transition $R3c \rightarrow R\bar{3}c$, the second line at 80 K higher can be identified as the phase transition $R\bar{3}c \rightarrow R\bar{3}m$ earlier discovered in $Ca_9Yb(VO_4)_7$ (ref. 21) and recently confirmed by DTA in $Ca_9Y(VO_4)_7$.[23] Conductivity activation energies E_a in Table 3 are calculated according to Arrhenius equation:

$$\ln(\sigma T) = \ln A - E_a/kT \qquad (1)$$

where A – exponential factor, k – Boltzmann constant. It is worth noting that the phase transitions only slightly affect the ionic conductivity of the crystals. Nevertheless, the data in Fig. 7 clearly demonstrate that the impact of temperature resulting in the symmetry increase in series $R3c \rightarrow R\bar{3}c \rightarrow R\bar{3}m$ is always accompanied by an enhancement of ionic conductivity.

4. Discussion

It is commonly known that even small amounts of guest atoms can drastically influence the optical and electrical

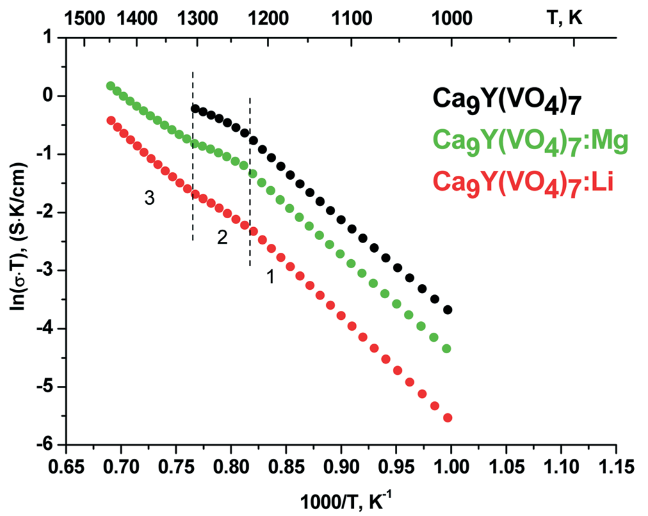

Fig. 7 The Arrhenius plot of electric conductivity for crystals $Ca_9Y(VO_4)_7$, $Ca_9Y(VO_4)_7$:Mg and $Ca_9Y(VO_4)_7$:Li in temperature regions of phases of different symmetry (1 – $R3c$, 2 – $R\bar{3}c$, 3 – $R\bar{3}m$).

Table 3 Electrical-conductivity activation energy E_a and dc-electrical conductivity σ for $Ca_9Y(VO_4)$ single crystals in high-temperature region in phases of different symmetry

	E_a, eV			$\sigma \times 10^{-4}$, S cm^{-1}		
Crystal	$R3c$	$R\bar{3}c$	$R\bar{3}m$	1150 K	1300 K	1400 K
C1	1.33	0.85	—	3.521	12.4	—
C2	1.58	1.03	1.52	0.457	2.73	4.18
C3	1.45	0.77	1.18	1.924	6.729	13

properties of many non-linear crystals. For example, magnesium-doped lithium niobate has better optical uniformity and is more resistant to optical damage in comparison with both stoichiometric and congruent-melt $LiNbO_3$ crystals.[28,29] However, mechanisms of such positive influence in different families of crystals are very different and must be disclosed in special investigations. The family of crystals $Ca_9R(VO_4)_7$ (R –REE or Bi) with whitlockite-type structure demonstrate a whole combination of technically important properties including lasing, optical non-linearity, ferroelectricity and ionic conductivity. In order to control the properties, a crystal-chemistry model of ferroelectric phase transitions has been already proposed,[7] and possible pathways for divalent calcium ion conduction considered.[30] There is direct evidence that ferroelectricity, ion-conductivity and related properties in the family are strongly influenced by inclusions of both guest atoms and defects. All of these inclusions distort the ideal crystal structure. In order to evaluate the real performance of Czochralski-grown $Ca_9Y(VO_4)_7$, a number of techniques have been employed to demonstrate the close relationship between crystal and real structures.

In whitlockite-type structures, Schottky type point defects may be easily produced due to the widely spread partial occupation of M4 cation positions. Moreover, structural defects may also appear due to statistical arrangement of different cations in sites M1–M3 and M5. For example, such defects were isolated and visualized in solid solutions of $Sr_{9+x}Ni_{1.5-x}(PO_4)_7$ ($R\bar{3}m$, $0.14 \le x \le 0.39$)[31] isostructural with β-$Ca_3(PO_4)_2$; both positional and orientational disorders were found in this material. Leonidov *et al.*[30,32] proved that the conductivity in REE-calcium vanadates only exists due to the mobility of calcium cations. The mobility of calcium cations has been found in $Ca_9ZnLi(PO_4)_7$ (ref. 33) and many other vanadates.[34]

According to the results of structural refinement in ref. 23, the Mg-containing crystal had a chemical formula $Ca_{8.84}Mg_{0.15}Y_{1.01}(VO_4)_7$. This formula corresponds to direct chemical analysis giving $Ca_{8.854}Mg_{0.145}Y(VO_4)_7$. It was found in ref. 23 that smaller magnesium atoms replaced part of the larger Ca atoms at their octahedral sites M5. Consequently, all lattice parameters adopt smaller values. A slightly contracted Mg-substituted lattice has a unit cell volume V = 3875.36 Å^3 which is smaller relative to 3881.65 Å^3 for $Ca_9Y(VO_4)_7$. Evidently, this makes the channels of Ca^{2+} ionic conductivity narrower in the crystal and results in a smaller electrical conductivity of the Mg-doped crystal in comparison with $Ca_9Y(VO_4)_7$ at any temperature (Fig. 7).

With respect to this, we cannot continue and connect the lowest conductivity in the $Ca_9Y(VO_4)_7$:Li^+ crystal with further shrinkage of ion-conducting channels, as far as in this case the unit cell volume appears to be much larger, V = 3880.77 Å^3, and is compatible with that of $Ca_9Y(VO_4)_7$. The most probable explanation for low conductivity leads us to assume that lithium atoms partly occupy the M4 position which is generally empty in $Ca_9Y(VO_4)_7$. When empty, this position works as a cross-point for 6 ion-conducting pathways,[11] therefore, its partial blocking by a guest atom may greatly diminish Ca^{2+}-conductivity. Taking into account the electroneutrality of the crystal lattice and structurally determined absence of heavy atoms in M4, the formula $Ca_{8.93}Li_{0.14}Y(VO_4)_7$ was derived. This formula has a simple structural interpretation: all atoms of lithium are in M4 and all heavy atoms are randomly distributed between M1–M3 and M5. Because of the low scattering power of lithium, the latter atoms could not be detected in M4 during X-ray structural characterization.[23] Nevertheless, it is known that insertion of lithium in the whitlockite-type substances already results in Li-atom locations exactly in the M4 site.[34] The M1–M3 and M5 sites may be partly populated with yttrium, rare-earth elements, or bismuth. In our Czochralski growth from the Li-enriched melt, the obtained crystal very likely results in a solid solution of $Ca_9Y(VO_4)_7$ and $Ca_{10}Li(VO_4)_7$. The changes in lattice parameter values with respect to $Ca_9Y(VO_4)_7$ follows the expected trends (see the $Ca_{10}Li(VO_4)_7$ data in Table 2).[23]

Along with the formation of solid solutions, the growth of single crystals from melts may be accompanied by the appearance of structural imperfections of different kind, mostly connected with chemical and temperature instabilities of the melt. In majority of cases, such imperfections are manifested in the local deformations of the crystal lattice and may be observed at the reciprocal lattice-point maps. The elliptical shape of the symmetrical 0 0 30 reflections in the RSMs proves that the crystals **C1** and **C3** exhibit a micromosaic structure and a homogeneous composition. For the Mg-doped specimen (crystal **C2**), both the shape of the node at the RSMs and the presence of the diffuse scattering indicate the presence of microdefects (inclusions/clusters).

Better optical transmittance and uniformity of crystals **C1** and **C3** observed by X-ray diffraction are in line with the result of dielectric measurements. Only sharp dielectric peaks $\varepsilon(T)$ were detected at temperatures of ferroelectric phase transitions, T_c, regardless if the specimen was cut either from top, medium or bottom parts of the crystal boule. For the Mg-doped sample (crystal **C3**), the higher amplitude of the ferroelectric peak (Fig. 4) gives additional evidence of a relatively worse structural uniformity of this crystal. In all the crystals, the ferroelectric phase transition is preceded by a $\tan\delta(T)$ maximum (Fig. 6). This anomaly is known to correspond to ferroelectric domain structure, which becomes switchable when the temperature approaches T_c. The ferroelectric Curie temperatures, T_c, for pure Mg- or Li-doped $Ca_9Y(VO_4)_7$ differ insignificantly around an averaged value of T_1 = 1213 ± 5 K. This temperature is close to the ferroelectric transition found in $Ca_9Yb(VO_4)_7$ single crystals at 1221 K in ref. 21.

5. Conclusions

Large (volume ≥1 cm^3) whitlockite-type single crystals were successfully grown by the Czochralski method from nominally pure, lithium- or magnesium-doped melts of whitlockite-type calcium-yttrium vanadate, $Ca_9Y(VO_4)_7$. Chemical analysis, X-ray structural and topographic investigations of corresponding crystals indicated that these crystals are clearly different in unit cell parameters, structural imperfections and impurity composition. Along with stoichiometric $Ca_9Y(VO_4)_7$, two other crystals include lithium or magnesium as guest atoms in amounts corresponding to chemical formulae $Ca_{8.93}Li_{0.14}Y(VO_4)_7$ and $Ca_{8.854}Mg_{0.145}Y(VO_4)_7$, thus representing solid solutions of the inclusion and substitution types, respectively. In these various crystals $Ca_9Y(VO_4)_7$, low content of guest atoms have very little impact on the ferroelectric Curie temperatures (1213 ± 5 K) as well as higher-temperature structural phase transitions in crystals. However, lithium atoms strongly reduce the Ca^{2+}-ionic conductivity of the crystals while the influence of magnesium is significantly less. Lithium-doped crystals gave the perfect reciprocal space map and demonstrated the best structural and optical quality.

Conflicts of interest

There are no conflicts to declare.

Acknowledgements

This research was supported by the Russian Science Foundation (Grant 16-13-10340).

Notes and references

1 S. Haussuhl and J. Liebertz, *Z. Kristallogr.*, 1978, **148**, 87–93.
2 A. M. Glass, S. C. Abrahams, A. A. Ballman and G. Loiacono, *Ferroelectrics*, 1977, **17**, 579–582.
3 P. S. Bechthold, J. Liebertz and U. Deserno, *Opt. Commun.*, 1978, **27**, 393–398.
4 L. Li, H. M. Noh, B. K. Moon, J. H. Jeong, B. C. Choi and X. Liu, *Opt. Mater. Express*, 2014, **4**, 16–28.
5 X. Wu, Y. Huang, L. Shi and H. J. Seo, *Mater. Chem. Phys.*, 2009, **116**, 449–452.
6 A. A. Belik, S. Y. Stefanovich and B. I. Lazoryak, *Mater. Res. Bull.*, 2001, **36**, 1873–1880.
7 B. I. Lazoryak, O. V. Baryshnikova, S. Y. Stefanovich, A. P. Malakho, V. A. Morozov, A. A. Belik, I. A. Leonidov, O. N. Leonidova and G. Van Tendeloo, *Chem. Mater.*, 2003, **15**, 3003–3010.
8 Z. Lin, G. Wang and L. Zhang, *J. Cryst. Growth*, 2007, **304**, 233–235.
9 N. Zhuang, X. Liu, Q. Xu, X. Chen, B. Zhao, X. Hu and J. Chen, *J. Alloys Compd.*, 2014, **595**, 113–119.
10 X. Hu, X. Chen, N. Zhuang, R. Wang and J. Chen, *J. Cryst. Growth*, 2008, **310**, 5423–5427.
11 S. Y. Stefanovich, D. A. Petrova, V. A. Morozov, E. A. Fortalnova, D. A. Belov, D. V. Deyneko, O. V. Barishnikova, A. A. Belik and B. I. Lazoryak, *J. Alloys Compd.*, 2018, **735**, 1826–1837.
12 D. V. Deyneko, S. Y. Stefanovich, A. V. Mosunov, O. V. Baryshnikova and B. I. Lazoryak, *Inorg. Mater.*, 2013, **49**, 807–812.
13 D. V. Deineko, S. Y. Stefanovich, A. V. Mosunov, O. V. Baryshnikova and B. I. Lazoryak, *Inorg. Mater.*, 2013, **49**, 507–512.
14 D. V. Deyneko, V. A. Morozov, J. Hadermann, A. E. Savon, D. A. Spassky, S. Y. Stefanovich, A. A. Belik and B. I. Lazoryak, *J. Alloys Compd.*, 2015, **647**, 965–972.
15 N. G. Dorbakov, V. V. Grebenev, V. V. Titkov, E. S. Zhukovskaya, S. Y. Stefanovich, O. V. Baryshnikova, D. V. Deyneko, V. A. Morozov, A. A. Belik and B. I. Lazoryak, *J. Am. Ceram. Soc.*, 2018, **101**, 4011–4022.
16 N. G. Dorbakov, O. V. Baryshnikova, V. A. Morozov, A. A. Belik, Y. Katsuya, M. Tanaka, S. Y. Stefanovich and B. I. Lazoryak, *Mater. Des.*, 2017, **116**, 515–523.
17 M. B. Kosmyna, P. V. Mateychenko, B. P. Nazarenko, A. N. Shekhovtsov, S. M. Aksenov, D. A. Spassky, A. V. Mosunov and S. Y. Stefanovich, *J. Alloys Compd.*, 2017, **708**, 285–293.
18 P. A. Loiko, A. S. Yasukevich, A. E. Gulevich, M. P. Demesh, M. B. Kosmyna, B. P. Nazarenko, V. M. Puzikov, A. N. Shekhovtsov, A. A. Kornienko, E. B. Dunina, N. V. Kuleshov and K. V. Yumashev, *J. Lumin.*, 2013, **137**, 252–258.
19 B. I. Lazoryak, A. A. Belik, S. Y. Stefanovich, V. A. Morozov, A. P. Malakho, O. V. Baryshnikova, I. A. Leonidov and O. I. Leonidova, *Dokl. Phys. Chem.*, 2002, **384**, 144–148.
20 W. Paszkowicz, A. Shekhovtsov, M. Kosmyna, P. Loiko, E. Vilejshikova, R. Minikayev, P. Romanowski, W. Wierzchowski, K. Wieteska, C. Paulmann, E. Bryleva, K.

Belikov and A. Fitch, *Nucl. Instrum. Methods Phys. Res., Sect. B*, 2017, **411**, 100–111.

21 B. I. Lazoryak, S. M. Aksenov, S. Y. Stefanovich, N. G. Dorbakov, D. A. Belov, O. V. Baryshnikova, V. A. Morozov, M. S. Manylov and Z. Lin, *J. Mater. Chem. C*, 2017, **5**, 2301–2310.

22 A. A. Belik, S. V. Grechkin, L. O. Dmitrienko, V. A. Morozov, S. S. Khasanov and B. I. Lazoryak, *Crystallogr. Rep.*, 2000, **45**, 13–20.

23 B. I. Lazoryak, D. V. Deyneko, S. M. Aksenov, S. Y. Stefanovich, E. A. Fortalnova, D. A. Petrova, O. V. Baryshnikova, M. B. Kosmyna and A. N. Shekhovtsov, *Z. Kristallogr. - Cryst. Mater.*, 2018, **233**, 453–462.

24 L. J. Farrugia, *J. Appl. Crystallogr.*, 1999, **32**, 837–838.

25 V. Petricek, M. Dusek and L. Palatinus, *Z. Kristallogr. - Cryst. Mater.*, 2014, **229**, 345–352.

26 M. B. Kosmyna, B. P. Nazarenko, V. M. Puzikov, A. N. Shekhovtsov, W. Paszkowicz, A. Behrooz, P. Romanowski, A. S. Yasukevich, N. V. Kuleshov, M. P. Demesh, W. Wierzchowski, K. Wieteska and C. Paulmann, *J. Cryst. Growth*, 2016, **445**, 101–107.

27 D. V. Deyneko, V. A. Morozov, S. Y. Stefanovich, A. A. Belik, B. I. Lazoryak and O. I. Lebedev, *Inorg. Mater.*, 2016, **52**, 176–185.

28 I. W. Kim, B. C. Park, B. M. Jin and E. Al, *Mater. Lett.*, 1995, **24**, 157–160.

29 L. Arizmendi, *Phys. Status Solidi A*, 2004, **201**, 253–283.

30 I. A. Leonidov, O. N. Leonidova, L. L. Surat and R. F. Samigullina, *Inorg. Mater.*, 2003, **39**, 616–620.

31 A. A. Belik, F. Izumi, T. Ikeda, V. A. Morozov, R. A. Dilanian, S. Torii, E. M. Kopnin, O. I. Lebedev, G. Van Tendeloo and B. I. Lazoryak, *Chem. Mater.*, 2002, **14**, 4464–4472.

32 I. A. Leonidov, M. Y. Khodos, A. A. Fotiev and A. S. Zhukovskaya, *Inorg. Mater.*, 1988, **24**, 280–281.

33 D. Wei, Y. Huang, J. S. Kim, L. Shi and H. J. Seo, *J. Electron. Mater.*, 2010, **39**, 441–446.

34 V. A. Morozov, I. A. Presnyakov, A. A. Belik, S. S. Khasanov and B. I. Lazoryak, *Crystallogr. Rep.*, 1997, **42**, 758–769.

